ChemPhysChem

Research Article
doi.org/10.1002/cphc.202400805

Chemistry Europe
European Chemical Societies Publishing

www.chemphyschem.org

Correlation Between Voltammetry of Immobilized Particles and Mott-Schottky Analysis of Metal Corrosion Patinas

Marta Porcaro,[a] Miguel Sanz-Abad,[b] Laura Michetti,[c] Alessandro Conti,[c] Caterina De Vito,[a] María Teresa Doménech-Carbó,[d] and Antonio Doménech-Carbó*[b]

The conjoint application of the voltammetry of immobilized particles (VIMP) methodology and the Mott-Schottky analysis (MS) of impedance data to studying metal corrosion patinas is described. The study is applied to copper and bronze objects exploiting the semiconducting character of cuprite and other copper corrosion products. A simplified theoretical modeling of MS analysis at microparticulate deposits extracted from metal corrosion layers attached to graphite electrodes is provided. The proposed model compensates for the disturbing effect of the regions of the basal electrode directly exposed to the electrolyte. Alternative models accounting for the variation of the density of charge carriers with depth are tested as well as the correlation between VIMP and MS data with reasonably satisfactory results.

Introduction

Electrochemical techniques play a prominent role in the analysis of solid materials.[1] Among them, the voltammetry of immobilized particles (VIMP) and Mott-Schottky (MS) analysis of impedance data have been extensively used to obtain compositional, thermochemical, and photochemical information. The former is of particular interest in the analysis of ion-insertion electrochemical processes[2–5] while the second has been largely exploited in the analysis of compact and nanostructured[6–8] semiconductor electrodes.

In principle, VIMP and MS deal with different electrochemical scenarios. VIMP involves studying faradaic processes occurring when reductive and/or oxidative potential inputs are applied to a microparticulate deposit of a solid material attached to an inert electrode in contact with a suitable electrolyte.[9–11] In contrast, MS analysis involves the record of the impedance response of a semiconductor film or a semiconductor compact electrode in contact with an electrolyte in conditions where no faradaic processes occur,[12–14] non-faradaic processes dominating the voltammetry of semiconductors.[15]

One of the fields in which VIMP and MS techniques can intersect is the analysis of metal corrosion patinas. In particular, the VIMP has been extensively used for the study of archaeological metal patinas,[16] involving the identification[17–19] and quantification[20] of components and screening of provenances, manufacturing techniques,[21–25] and age.[26] This technique is particularly useful in the archaeometric domain because it requires only a few nanograms of sample.[9–11,16] However, a common difficulty for acquiring physicochemical information is the stratified, often heterogeneous, nature of metal corrosion layers. In the case of copper-based objects under 'smooth' corrosion conditions, there is a primary cuprite patina covered by a secondary patina where cuprite can be accompanied by tenorite and other components,[27–29] the composition, compaction, porosity, crystallinity varying with depth.[30–32] In this context, a multiple-scan voltammetric strategy was developed to extract information on the in-depth properties of metal patinas.[33–35]

More recently, we have applied the MS technique to characterize archaeological metal patinas.[36] The essential idea was that, given the semiconducting nature of the usual copper corrosion products,[37,38] the changes in composition, compaction, crystallinity, etc. of the corrosion layers should be reflected in changes in the MS parameters recorded for representative samples of metal patinas attached to graphite electrodes using the abrasive sampling methodology characteristic of the VIMP. This procedure offers two difficulties: i) the separation of the contributions to the impedance response of the microparticulate deposit and the bare graphite electrode directly exposed to the electrolyte solution, and ii) the in-depth variation of the properties of the metal corrosion patina.

The current report describes a theoretical analysis of how the changes in composition, compaction, crystallinity, porosity, etc. of the metal patina are reflected in the faradaic voltammetric response associated with the reduction of the patina components, and in the MS response recorded under non-

[a] M. Porcaro, C. De Vito
Department of Earth Sciences, Sapienza University of Rome, P.le Aldo Moro 5, 00185 Rome, Italy

[b] M. Sanz-Abad, A. Doménech-Carbó
Department of Analytical Chemistry, University of Valencia, Dr. Moliner 50, 46100 Burjassot, Valencia, Spain
E-mail: antonio.domenech@uv.es

[c] L. Michetti, A. Conti
Department of Classics, Sapienza University of Rome, P.le Aldo Moro 5, 00185 Rome, Italy

[d] M. Teresa Doménech-Carbó
Institut de Restauració del Patrimoni, Universitat Politècnica de València, Camí de Vera 14, 46022 València, Spain.

Supporting information for this article is available on the WWW under https://doi.org/10.1002/cphc.202400805

faradaic conditions. As a result, different in-depth modes of VIMP and MS parameters can be obtained and correlated to predict experimentally testable relationships. Such testing was carried out using Eurocent coins and a set of archaeological samples from the Etruscan archaeological site of Pyrgi in Santa Severa (Rome, Italy). VIMP and MS data are complemented by electrochemical impedance spectroscopy (EIS) data aimed at selecting the optimal conditions (frequency, potential range) for MS analysis.

Experimental

Impedance and voltammetric measurements were performed at room temperature (251 °C ±) using a CH I920c potentiostat (Cambria Scientific, Llwynhendy, Llanelli UK) using a conventional three-electrode cell. The working electrodes consisted of sample-modified graphite bars (Faber-Castell HB type, diameter 2 mm). For sampling, the plane edge of the graphite bar, previously polished on paper,[9–11] was pressed over a flat area of the metallic object. The three-electrode arrangement was completed with a platinum wire auxiliary electrode and an Ag/AgCl (3 M NaCl) reference electrode. Electrochemical measurements were performed in air-saturated 0.25 M HAc/NaAc solution (Probus Reagents) at pH 4.75. EIS experiments were carried out at the open circuit potential (OCP) in the 0.1–10^5 Hz frequency range and an amplitude (peak-to-peak) of 10 mV, after an equilibration time of 5 min. MS analysis was performed at potentials between 0.0 and 1.0 V vs. Ag/AgCl at frequencies between 10^2 and 10^5 Hz. The validity of the impedance data was checked using, as usual, the Kramers-Kronig (K–K) transformation.[39] The sample-modified electrode surfaces were examined using field emission scanning electron microscopy (Model S-4800, Hitachi Ltd., Tokyo, Japan) operating at 20 kV.

Sampling was performed on Eurocent coins with different degrees of moderate aging, exhibiting from lustrous to opaque brown patinas. Concerning the archaeological samples, five nails recovered from the Etruscan archaeological site of Pyrgi in Santa Severa (Rome, Italy) were studied. The nails were recovered in different locations of the archaeological site covering ages between the first half of the 5th century BC and the end of the 6th century BC. The details about the location and other archaeological characteristics of the objects are given in Table 1. The sampling was performed on 3–5 areas of the surface of nails and coins selecting regions showing a smooth texture and uniform brownish/greenish color.

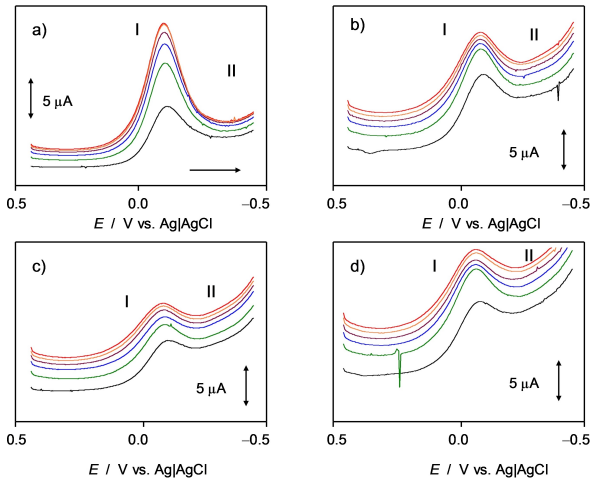

Figure 1. Square wave voltammograms recorded for graphite electrodes modified with samples a) 22, b) 52640, c) 31, and d) 9787 in contact with air-saturated 0.25 M HAc/NaAc aqueous solution at pH 4.75. The 1st to 6th successive potential scans are superimposed. Potential scan initiated at 0.25 V vs. Ag/AgCl in the negative direction; potential step increment 4 mV; square wave amplitude 25 mV; frequency 10 Hz. The horizontal arrow marks the direction of the potential scan.

Results and Discussion

VIMP Data

Figure 1 shows the net square wave voltammograms of graphite electrodes modified with samples 22, 52640, 31, and 9787 in contact with 0.25 M acetate buffer at pH 4.75. The voltammograms were recorded by scanning the potential in the negative direction and are represented as net current/potential curves. The net current corresponds to the difference between the forward (cathodic) and backward (anodic) components. The voltammograms show the typical response displayed by copper/bronze corrosion patinas,[21–26] consisting of an intense cathodic peak ca. −0.10 V vs. Ag/AgCl (I) followed by a more or less defined shoulder ca. −0.4 V (II). The signal I can be assigned to the reduction of cuprite (Cu_2O), eventually superimposed to the reduction of minerals of the atacamite, brochantite and/or malachite groups, to copper metal, while process II can be assigned to the corresponding tenorite (CuO) to copper reduction.[21–26]

This voltammetry is in agreement with previous studies.[21–26] If the potential range is extended to more negative values, a broad cathodic peak appears ca. −0.75 V, corresponding to the reduction

Table 1. Table Caption. List of archaeological objects handled in this study. All correspond to finds of the Etruscan civilization from the archaeological site of Pyrgi (Santa Severa, Rome).

Inventory number	Typology	Provenance	Period
22	Nail	South Sanctuary, North Square	5th century BC
31	Nail	South Sanctuary, North Square	5th century BC
52640	Nail	Monumental Sanctuary, Temple B	End of the 6th century BC
9787	Nail	Monumental Sanctuary, Temple A	First half of the 5th century BC
04bV57	Nail	South Area, beta building	5th–4th century BC

of dissolved oxygen (oxygen reduction reaction, ORR). This signal precedes the rising current representative of the hydrogen evolution reaction (HER), as is depicted in Figure S1 in Supplementary Information. In solutions deaerated by bubbling Ar, the ORR signal disappears. Progressive re-oxygenation of the electrolyte solution results in the progressive increase and positive shift of the ORR (see data for a controlled aeration experiment depicted in Figure S2, Supplementary Information). Since this process occurs at potentials where the corrosion compounds have been reduced to copper metal, these features suggest that it produces some catalytic effect on the ORR.

Under the same experimental conditions, sample-modified electrodes do not show any faradaic signal when the potential is scanned between 0.0 and 0.8 V (see Supplementary Information, Figure S1). Accordingly, this potential range is potentially available for performing impedance measurements to be applied for MS analysis.

Impedance Data

Figure 2a shows the Nyquist plot of the impedance spectrum recorded for sample 9787-modified graphite electrode in contact with 0.25 M HAc/NaAc buffer at pH 4.75. The experiments were conducted at the open-circuit potential (OCP) previously measured. In all cases, values between 0.10 and −0.10 V vs. Ag/AgCl were recorded. Here, the (minus) imaginary component of the total impedance ($-Z_{imag}$) is plotted vs. the real component of the total impedance (Z_{real}). The representation corresponds to a depressed loop at middle and low frequencies preceded by a small semicircle at high frequencies whereas the total impedance vs. log(frequency) plot shows the usual s-shaped curve (see Figure 2b). The Bode plot of the (minus)phase angle ($-\varphi$) vs. log(frequency) (log*f*) in Figure 2c shows two ill-defined maxima at high and low frequencies. Similar spectra were obtained for all other samples. Such spectra can be reproduced satisfactorily by the equivalent circuit depicted in Figure 2d. In this circuit, R_s represents the solution resistance whereas R_{ct} and C_{dl} can be attributed to the charge transfer resistance and the double-layer capacitance associated with the interface between the exposed graphite surface and the electrolyte solution. The charge transfer resistance is representative of the energy barrier for charge transfer existing at the interface electrode/electrolyte. These elements are placed in parallel between them and connected in series with R_s and a second parallel RC couple. This RC unit can be taken as representative of the resistive (R_p) and capacitive effects associated with the ensemble of metallic sheets adhered to the graphite surface. The best fit of the data was obtained by inserting a constant phase element (Q_p) as representative of the non-ideality of the above capacitive effect. Impedance spectra recorded at unmodified graphite electrodes (see Figure S3 in Supplementary Information) show a qualitatively similar pattern. This is consistent with the large proportion of graphite surface directly exposed to the electrolyte solution in sample-modified electrodes. The spectra of unmodified electrodes can be modeled by replacing the constant phase element with a capacitor. Comparison of EIS data for sample-modified and unmodified electrodes suggests that the optimal frequency for MS analysis is between 10^2 and 10^4 Hz where, as can be seen in Figure 2c, the larger capacitive effects appear.

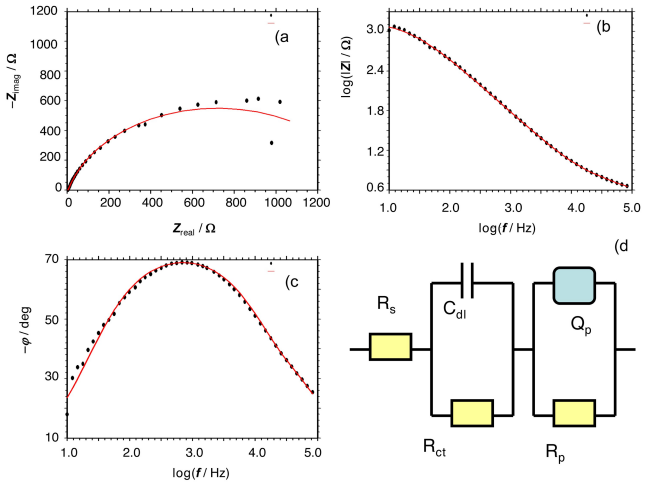

Figure 2. Impedance spectrum recorded for sample 9787 at the OCP in contact with 0.25 M HAc/NaAc aqueous buffer at pH 4.75. a) Nyquist plot of (minus)Z_{imag} vs. Z_{real}; b) detail of the high-frequency region of the Nyquist plot; c) Bode plot of (minus)phase angle vs. log*f*; d) Equivalent circuit used for simulation. Experimental data points (black circles) are superimposed to the theoretical spectrum (red lines) taking $R_s = 5\ \Omega$, $C_{dl} = 3.1\ \mu F$, $R_{ct} = 10\ \Omega$, $R_p = 1430\ \Omega$, $Q_p = 11.4\ \mu\Omega s^{-n}$ ($n = 0.83$).

Figure 3 shows MS plots obtained after impedance measurements at graphite electrodes modified with samples extracted from the patina of a 'fresh' Eurocent coin in contact with 0.25 M HAc/NaAc buffer at pH 4.75 at frequencies of 10^3 and 10^4 Hz. The potential was initiated at 0.05 V vs. Ag/AgCl and scanned in the positive direction. The MS representations are divided into two regions. At potentials between 0.25 and 0.80 V experimental data points can be fitted to a straight line of negative slope (notice that the potential axis is inverted in Figure 3 to accommodate the scale used in voltammetric measurements). The negative MS slope is in agreement with the expectances resulting from the recognized *p*-type semiconducting behavior of cuprite, the main corrosion product of copper. However, in the region between 0.05 and 0.25 V, experimental data appear to define an opposite tendency.

These features can be interpreted on considering that when equilibrium is established between a semiconductor and an electrolyte, the Fermi level in the semiconductor and the redox potential of the electrolyte must be equalized via charge transfer between them. The excess charge in the semiconductor resides in a space charge region responsible for MS capacitive effects associated with the mobility of charge carriers.[40–45] According to the point defect model,[42] in the case of TiO_2, a *n*-type semiconductor, the semiconducting behavior is mainly associated with anion vacancies. For

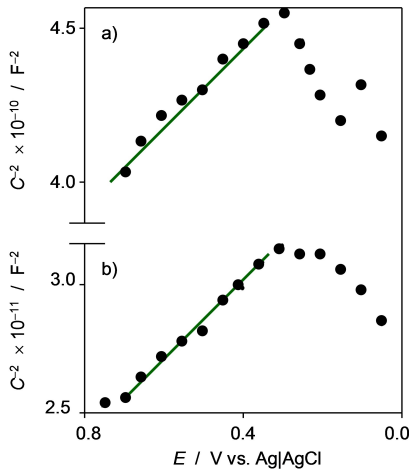

Figure 3. MS plots of C^{-2} vs. applied potential for 'fresh' Eurocent-modified graphite electrodes in contact with 0.25 M HAc/NaAc aqueous buffer at pH 4.75. Potentials initiated at 0.05 V vs. Ag/AgCl in the positive direction, frequency a) 10^3 Hz, b) 10^4 Hz.

reasons of charge conservation, these are associated with Ti(III) sites in the solid lattice. In the case of cuprite, a *p*-type semiconductor, the semiconducting behavior is mainly associated with cation vacancies. These must be associated with Cu(II) centers in the cuprite lattice. It is pertinent to note that the concentration and diffusivity of charge carriers are significantly potential-dependent.[40] This is reflected, in data reported for the MS analysis of cuprite[40,41] and other[42,43] metal oxide layers, including bronze patinas[44] where the oxide layers show both *p*-type and *n*-type semiconducting behavior depending on the applied potential.

Experiments at the bare graphite electrode showed a less-defined response corresponding to a *p*-type semiconducting behavior at potentials between 0.5 and 0.8 V (see Figure 4). This semiconducting behavior has been studied in detail for graphene oxide and reduced graphene oxide. In these materials, this behavior has been associated with the presence of surface oxygenated functions.[46,47] This semiconductor character can be extended to the 'ordinary' graphite in which semiconducting areas have been characterized.[48] Comparison of the MS slopes determined at unmodified and sample-modified electrodes revealed significant differences in the

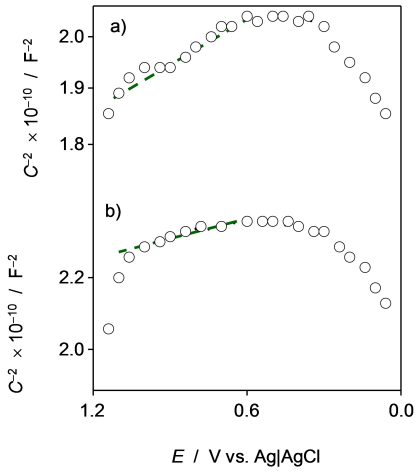

Figure 4. MS graph recorded at frequencies of a) 10^3 Hz, and b) 10^4 Hz for an unmodified graphite electrode immersed into air-saturated 0.25 M HAc/NaAc aqueous solution at pH 4.75. Potentials initiated at 0.05 V vs. Ag/AgCl in the positive direction. The dotted lines mark the linear region associated with a p-type semiconducting behavior.

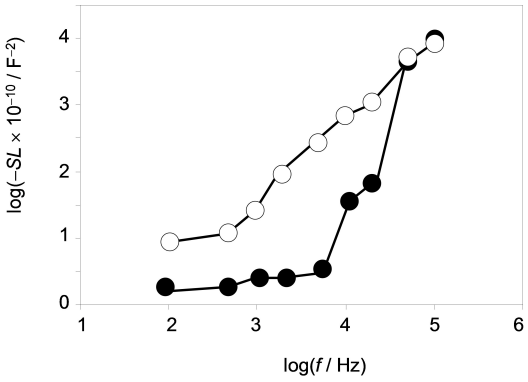

Figure 5. Variation with the frequency on the slope (SL) of the MS plots recorded from impedance data at unmodified (solid circles) and Eurocent-modified (circles) graphite electrodes in contact with air-saturated 0.25 M HAc/NaAc aqueous solution at pH 4.75. A logarithmic plot has been used for clarity.

interval of frequencies around 10^4 Hz (see Figure 5). Accordingly, MS experiments were carried out at this frequency.

These frequency-dependent differences can be rationalized in terms of differences in the spatial distribution of the density of electronic states in semiconductors.[8] The electrons in the band gap suffer a delay to follow the fluctuation of an externally applied electrical field, the time constant for this response increasing exponentially with the distance from the bottom of the conduction band.[49,50] For practical purposes, this can be interpreted as assuming that the MS graphs reflect the response of the semiconductor at a given depth that depends on the frequency of the exciting field. The result is that the Mott-Schottky response of different semiconducting materials varies differently with the applied frequency.[51,52]

VIMP Modeling

As described already in detail,[33] the VIMP sampling results in a deposit of *k* sheets of micrometric size adhered to the base graphite electrode. These sheets were extracted from the corrosion layers of the metal objects so under the application of reductive potential inputs become progressively delaminated. Given the geometry of the sampling process schematized in Figure S4 in Supplementary Information, the delamination starts from the more external layer of the corrosion patina[33–35] because, as described in VIMP modeling,[10,53–55] the electrochemical reaction starts at the solid particles/base electrode/electrolyte solution three-phase junction.

For simplicity, we will assume that a series of *k* sheets of average area *S*, and average thickness δ constitute the deposited sample. Application of the first cathodic scan will result in the removal of a lamina of thickness $z(1) < \delta$. Assuming that the corrosion layers are constituted by a homogeneous distribution of cuprite, the net charge passed in the initial cathodic scan, $q(1)$, determined from the area under the voltammetric peaks, will be,

$$q(1) = gkS\rho(1)z(1) \tag{1}$$

where $\rho(1)$ represents the average cuprite density in the layer and *g* is an electrochemical constant that remains constant for fixed experimental conditions. A more realistic approach assumes that crystallinity, compaction, etc. of cuprite patina vary with depth.[30–32] Then, the charge passed in the initial cathodic scan will be,

$$q(1) = gkS \int_{z=0}^{z(1)} \rho(z)dz \tag{2}$$

where $\rho(z)$ is the function (assumed to be continuous) representative of the variation of cuprite density with depth, and $z(1)$ is the thickness of the lamina removed in the first scan. If successive cathodic scans are applied resulting in the reductive dissolution of cuprite and formation of an external deposit of copper metal, the accumulated charge after *N* scans, $Q(N)$, will be,

$$Q(N) = q(1) + q(2) + \ldots q(N) = gkS \int_{z=0}^{z(N)} \rho(z)dz \tag{3}$$

Then, the $q(1)/Q(N)$ ratio will be independent of the number and averaged area of the patina sheets:

$$\frac{q(1)}{Q(N)} = \frac{\int_{z=0}^{z(1)} \rho(z)dz}{\int_{z=0}^{z(N)} \rho(z)dz} \quad (4)$$

It is pertinent to note that square wave voltammograms reflect the difference current between the measured forward and backward currents sampled at the end of potential pulses. Then, difference peak currents and areas do not represent the exact charge exchanged during the electrochemical process. As already discussed in detail,[33] in our systems a large proportion of the electrode surface consists of graphite directly exposed to the electrolyte solution. Under these circumstances, the contribution of background currents could be significant in both forward and backward square wave components, but this contribution can be taken as quite similar at the end of both forward and backward potential pulses. Accordingly, the background contribution can be assumed to cancel out in the net (difference) current. Then, square wave difference currents can be reasonably taken as representative of charges passed in the corresponding electrochemical processes.[33]

MS Modeling

The Mott-Schottky equation describes the variation of the space charge capacity (C_{SC}) of a homogeneous film of a semiconducting material in contact with an electrolyte with the applied potential (E) when no faradaic processes take place. For a compact semiconducting electrode, the relationship between C_{SC} (F) and E (V) is expressed as depending on the density of charge carriers, N_D (cm^{-3}), and the flat band potential, E_{FB} (V), as,

$$\frac{1}{C_{SC}^2} = \pm\frac{2}{N_D \varepsilon S^2 e}\left(E - E_{FB} - \frac{k_B T}{e}\right) \quad (5)$$

In this equation e is the electron charge, S is the electrode area (cm^2), k_B is the Boltzmann constant, and ε (F cm^{-1}) is the permittivity of the material. The latter quantity is usually expressed as the product of the vacuum permittivity, ε_o, ($= 8.854\times10^{-14}$ F cm^{-1}), and the relative permittivity (the 'dielectric constant') of the material, ε'. The MS equation predicts a linear variation of $1/C_{SC}^2$ with E. The slope of the corresponding representation is positive for a n-type semiconductor or negative for a p-type semiconductor. For simplicity, we will always refer to the absolute value of the MS slope and rewrite the MS equation as,

$$\frac{1}{C_{SC}^2} = \frac{A}{S^2}(E - B) \quad (6)$$

where $A = 2/e\varepsilon N_D$ and $B = E_{FB} + k_B T/e$. In conventional MS analysis, it is assumed that the space charge capacitance is accompanied in series by the double layer capacitance (C_{dl}) at the semiconductor-electrolyte solution interface. This is usually of 2–3 orders of magnitude larger than C_{SC}, so that, in practice, the contribution of the double-layer capacitance can be neglected. However, our system is constituted, as evidenced by electron microscopy images of sample-modified electrodes,[33] by a series of sheets of micrometer size, extracted from the corrosion layers of the metal object, and deposited onto the graphite surface. Figure 6 shows the scanning electron microscopy (SEM) images of a metallic sheet over the base graphite electrode (a), and the surface of a patina sheet (b). One can see that the patina sheets extracted from metal objects

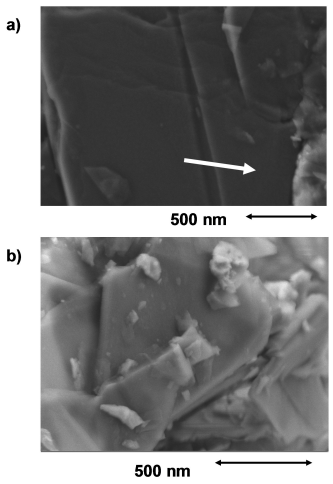

Figure 6. SEM images of a graphite electrode after sampling on a Eurocent coin. a) Image of the base graphite close to a patina sheet (marked by an arrow). B) Image of the upper surface of a patina sheet.

form a series of superimposed crystals adhered to the smoother graphite terraces.

A simplified modeling of this system is schematized in Figure 7a. This idealized view implies that there are three charge transfer pathways: a) directly between the electrolyte and the exposed bare graphite surface, b) through the sheet/electrolyte interface, and c) through the three-phase solid sheet/graphite/electrolyte boundary. At sufficiently cathodic potentials, charge transfer occurs preferentially through the three-phase boundary giving rise to faradaic processes occurring in VIMP experiments shown in Figure 1. At clearly higher potentials, there is no place for such faradaic processes and only the processes of semiconductor/electrolyte equilibration/polarization previously described will take place. This results in the 'ordinary' p-type MS behavior illustrated in Figures 3 and 4. At intermediate potentials, capacitive charging effects determine the 'anomalous' n-type MS behavior also recorded in these figures.

The description of the ordinary MS response implies the incorporation of the double-layer capacity of the electrolyte solution/'free'

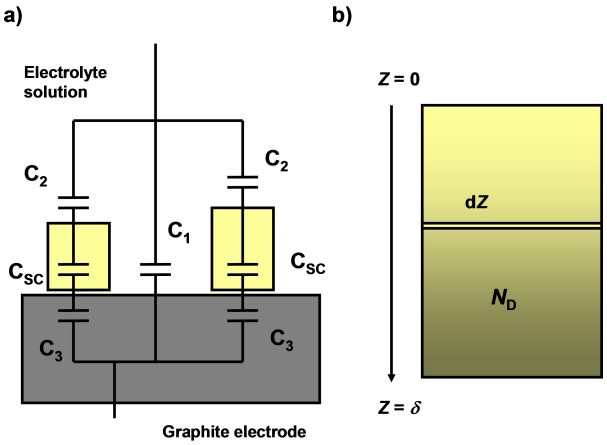

Figure 7. a) Scheme of the capacitive terms involved in the impedance measurements of sample-modified graphite electrodes in contact with an electrolyte solution. b) Idealized representation of a metallic sheet from the corrosion layer of a metal object assumed to be constituted by cemented grains.

graphite interface (C_1 in the figure). Strictly, the entire capacitive set must include the above-mentioned double-layer capacity at the metal sheets-electrolyte solution interface (C_2 in the figure) and the capacity at the graphite/metal sheet interface (C_3 in Figure 4a). Since C_{SC}, C_2, and C_3 are in series, the inverse of the total capacitance is the sum of their reciprocals. In the most favorable case, $C_{SC} \ll C_2$, C_3, and the contribution of C_2 and C_3 to the measured capacity will be negligible.

However, the capacity C_1 is in parallel with C_{SC}. Ideally, if the modified electrode contains k identical sheets of thickness δ, the total capacity will be,

$$C = kC_{SC} + C_1 \quad = \frac{kS}{\sqrt{A(E-B)}} + C_1 \tag{7}$$

Since, in principle, the contribution of C_1 to the measured capacity will not be negligible, our impedance measurements do not reflect immediately the space charge capacitance of the sheets. Then,

$$\frac{1}{C^2} = \frac{1}{\frac{k^2S^2}{A(E-B)} + 2\frac{kSC_1}{\sqrt{A(E-B)}} + C_1^2} \tag{8}$$

On first examination, C_1 can be taken as the double-layer capacitance which appears at the graphite directly exposed to the electrolyte solution. Since the total area of patina sheets is much lower than the total area of the graphite electrode,[33–35] C_1 can be considered as a constant. Depending on the values of A, B, and C_1, we can distinguish three regions in the variation of $1/C^2$ on E. For large values of C_1, $1/C^2$ is independent of E. In turn, for middle values of C_1, $1/C^2$ tends to,

$$\frac{1}{C^2} \approx \frac{\sqrt{A(E-B)}}{2kSC_1} = \frac{\sqrt{\frac{2}{N_D\varepsilon e}(E - E_{FB} - k_BT)}}{2kSC_1} \tag{9}$$

corresponding to a linear variation of $1/C^2$ on the square root of $E - B$. Finally, for small values of C_1, Equation (8) approaches to,

$$\frac{1}{C^2} = \frac{1}{\frac{k^2S^2}{A(E-B)}} = \frac{2}{k^2S^2N_D\varepsilon e}(E - E_{FB} - k_BT/e) \tag{10}$$

This corresponds to a linear variation of $1/C^2$ on E whose slope (SL) and ordinate at the origin (OO) are, respectively,

$$SL = \frac{2}{k^2S^2N_D\varepsilon e} \tag{11}$$

$$OO = -\frac{2(E_{FB} + k_BT/e)}{k^2S^2N_D\varepsilon e} \tag{12}$$

These quantities depend on the number of sheets, k, and their area, S. The abscissa at the origin (AO), however, is independent of such quantities,

$$AO = -(E_{FB} + k_BT/e) \tag{13}$$

In replicate sampling experiments on metallic corrosion layers, the number (and area) of the patina sheets transferred onto the graphite electrode surface varies. Then, different linear $1/C^2$ vs. E plots differing in slopes and intercepts will be obtained. However, they should verify a linear relationship:

$$OO = -(E_{FB} + k_BT/e)SL \tag{14}$$

A refined approach assumes that C_1 contains not only the double-layer capacitance of the graphite/electrolyte solution interface but also some semiconducting contribution associated with the graphite. Ideally, Equation (7) can be rewritten as,

$$C = \frac{kS}{\sqrt{A(E-B)}} + \frac{1}{\sqrt{G(E-H)}} \tag{15}$$

where G and H are the graphite counterparts of the Mott-Schottky parameters A and B. Then, Equation (8) becomes,

$$\frac{1}{C^2} = \frac{1}{\frac{k^2S^2}{A(E-B)} + 2\frac{kS}{\sqrt{AG(E-B)(E-H)}} + \frac{1}{G(E-H)}} \tag{16}$$

This equation can be approximated by a linear dependence of $1/C^2$ on E where, as before, the slope and the intercept will depend on the number and surface area of the patina sheets transferred onto the graphite electrode surface. Accordingly, if we perform different sampling processes on the same corroded object with different pressures (conceivably extracting sheets of different thicknesses), the values of OO and SL should display a linear relationship of the type,

$$OO = -R(SL) + T \tag{17}$$

R and T being case-sensitive parameters.

A more realistic description of the corrosion layers involves their view as constituted by an ensemble of cemented grains, i.e., a nanostructured material. In this case, the MS equation must be treated differently, now resulting in a variable flat band potential.[7] Additionally, if intergranular corrosion occurs, intergranular capacitances should be accounted for.[34,35] For simplicity, let us assume that the composition, compactness, porosity, etc. vary through each patina sheet as schematized in Figure 7b. Accordingly, the MS equation for an individual sheet of area S when the impedance response corresponds to a region of thickness δ can be rewritten as,

$$\frac{1}{C_{SC}^2(\delta)} \quad = \quad \pm\frac{2}{\varepsilon(\delta)N_D(\delta)S^2e}(E - E_{FB}(\delta) - k_BT/e) \tag{18}$$

Here, $\varepsilon(\delta)$, $N_D(\delta)$, $E_{FB}(\delta)$, represent the respective properties averaged to the assumed continuous variation of each property with depth z, i.e., $N_D = N_D(z)$, $E_{FB} = E_{FB}(z)$, and $\varepsilon = \varepsilon(z)$. This means that, after different sampling experiments on the same corroded object, the corresponding MS plots could diverge from linearity. Since our experimental data reveal the maintenance of satisfactory linear MS plots, it is reasonable to assume that there is a smooth variation of the semiconducting properties with depth in the corrosion patina. On first examination, it seems reasonable to assume that both $E_{FB}(z)$ and $\varepsilon(z)$ can be treated as constants, being the density of charge carriers (electrons for n-type semiconductors, holes for p-type semiconductors) the quantity most sensitive to changes in depth. Then, the MS equation can be rewritten in terms of an averaged density of charge carriers given by,

$$N_D(\delta) \approx \frac{\int_{z=0}^{z=\delta} N_D(z)dz}{\delta - 0} \quad (19)$$

One plausible possibility is that N_D decreases exponentially from the primary patina/secondary patina boundary located at a depth z_{inn}. This can be expressed as,

$$N_D(z) = N_D^{inn} e^{-a(z-z_{inn})} \quad (20)$$

a being a constant and N_D^{inn} the density of charge carriers at the primary patina/secondary patina boundary. In this model, the coefficient a is that $N_D e^{az_{inn}}$ equals the density of charge carriers at the external surface ($z=0$). N_D^{ext}. Assuming that the depth reached in the impedance measurement, δ, is lower than z_{inn}, we obtain,

$$N_D(\delta) = \frac{1}{\delta}\int_{z=0}^{z=\delta} N_D^{inn} e^{-a(z-z_{inn})}dz = \\ = \frac{N_D^{inn}}{a\delta}\left(e^{a\delta} - e^{-a(\delta - z_{inn})}\right) \quad (21)$$

The slope of the MS plot will be,

$$SL(\delta) = \frac{2a\delta}{\varepsilon e N_D^{inn}\left(e^{a\delta} - e^{-a(\delta - z_{inn})}\right)} \quad (22)$$

Now, let us consider the frequency dependence of the semiconductor response studied by La Mantia et al..[8] The simplest approximation is that the screening (or penetration) depth δ is proportional to the characteristic time of the exciting signal, i.e., inversely proportional to the frequency f. Accordingly, introducing a proportionality constant r ($\delta = rf$), one obtains,

$$SL(\delta) = \frac{2a(r/f)}{\varepsilon e N_D^{inn}\left(e^{ar/f} - e^{-a(r/f - z_{inn})}\right)} \quad (23)$$

In the limiting case in which a was small, Equation (23) leads to predict the proportionality between $SL(\delta)$ and f^{-1}.

Now, let us assume that there is a potential variation of the density of charge carriers with depth represented as,

$$N_D(z) = N_D^{int} - (N_D^{inn} - N_D^{ext})\left[1 - \left(\frac{z}{z_{inn}}\right)^{\alpha}\right] \quad (24)$$

where N_D^{ext} represents the density of charge carriers at the external surface of the corrosion patina. Now, the average density in a layer of thickness δ is,

$$N_D(\delta) = \frac{1}{\delta}\int_{z=0}^{z=\delta}\left\{N_D^{int} - (N_D^{inn} - N_D^{ext})\left[1 - \left(\frac{z}{z_{inn}}\right)^{\alpha}\right]\right\}dz \quad (25)$$

i.e.,

$$N_D(\delta) = N_D^{ext} + \frac{N_D^{inn} - N_D^{ext}}{(1+\alpha)z_{inn}^{\alpha}}\delta^{\alpha} \quad (26)$$

and,

$$SL(\delta) = \frac{2}{\left[N_D^{ext} + \frac{N_D^{inn} - N_D^{ext}}{(1+\alpha)z_{inn}^{\alpha}}\delta^{\alpha}\right]\varepsilon e} \quad (27)$$

Assuming, as above, that the screening depth δ is inversely proportional to the frequency f, we can write,

$$SL(\delta) = \frac{2}{\left[N_D^{ext} + \frac{N_D^{inn} - N_D^{ext}}{(1+\alpha)z_{inn}^{\alpha}}(r/f)^{\alpha}\right]\varepsilon e} \quad (28)$$

When the density of charge carriers in the external surface of the patina is small, the above equation leads to the proportionality between $SL(\delta)$ and f^{α}.

$$SL(\delta) \approx \frac{2(1+\alpha)z_{inn}^{\alpha}}{\varepsilon e N_D^{inn} r^{\alpha}} f^{\alpha} \quad (29)$$

Experimental data are consistent with this prediction. As shown in Figure 8, corresponding to data taken at frequencies between 10^2 and 10^5 Hz for a moderately corroded Eurocent coin, the plot of log($SL(\delta)$) vs. log$f$ fits satisfactorily to a straight line of slope 1.25 at frequencies between 500 and 10^5 Hz.

Crossing VIMP and MS

As previously noted, the sampling process used in VIMP and MS experiments produces the adhesion of different net amounts of sample over the surface of graphite electrodes. Then, replicate experiments do not reproduce exactly the voltammetric or impedance pattern. This effect can be seen in Figure 9, where the variation of accumulated peak currents ($I_p(N) = i_p(1) + i_p(2) + \ldots i_p(N)$) for replicate measurements on samples extracted from object 31 with the scan number, N is depicted from voltammograms recorded in conditions such as utilized in Figure 1. As expected, sampling in different areas of the same object produced different series of data (as a result of the different amounts and different depths reached during sampling) of the sample transferred onto the graphite surface.

Figure 10 shows three MS plots recorded in replicate experiments on samples taken on the surface of object 22 in contact with

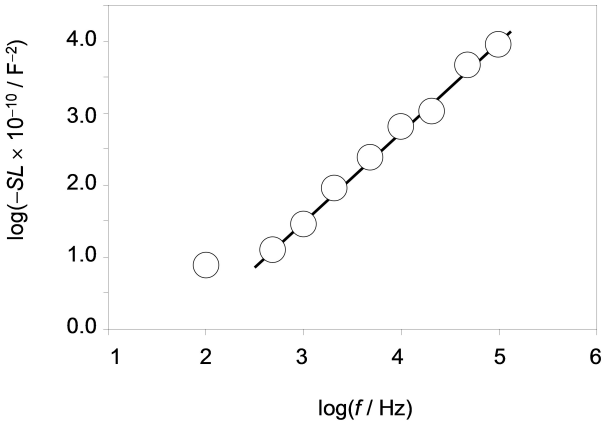

Figure 8. Plots of log(SL) vs. log$f$ for impedance data recorded for a Eurocent-modified graphite electrode in contact with air-saturated 0.25 M HAc/NaAc aqueous buffer at pH 4.75 at different frequencies in the potential range between 0.05 and 0.80 V vs. Ag/AgCl.

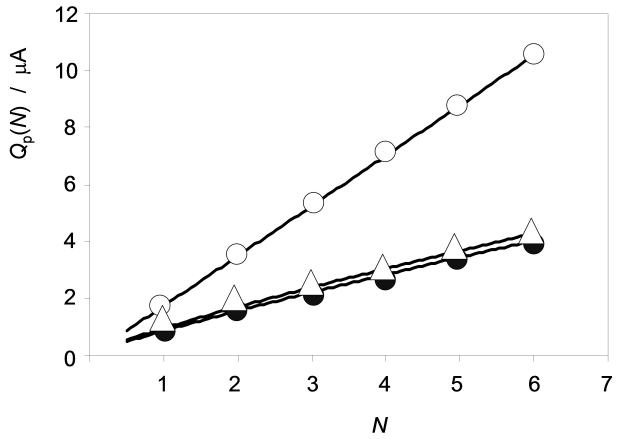

Figure 9. Plots of $I_p(N)$ vs. N for three independent VIMP measurements on sample 31 in conditions such as in Figure 1.

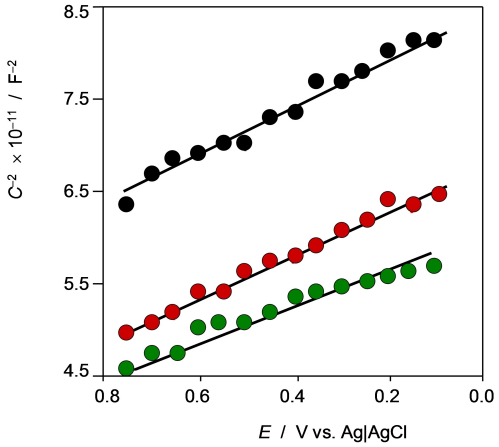

Figure 10. MS plots of C^{-2} vs. applied potential for graphite electrodes modified with object 22 aliquots in contact with air-saturated 0.25 M HAc/NaAc aqueous buffer at pH 4.75. Three independent measurements on samples taken from different points of the surface of the object are superimposed. Potentials initiated at 0.10 V vs. Ag/AgCl in the positive direction; frequency 10^4 Hz.

acetate buffer (see also Figure S5 in Supplementary Information). One can see that, in agreement with the expectances, different linear MS plots of negative slope are obtained in the potential range between 0.0 and 0.8 V. This denotes a *p*-type semiconducting behavior. The differences in replicate experiments result from the different net amounts of sample transferred onto the graphite electrode. Figure 11 depicts the plots of *OO* vs. *SL* from impedance data recorded in contact with acetate buffer at graphite electrodes modified upon sampling on 'fresh' and 'aged' Eurocent coins, and samples from objects 504bV57 and 52640. Such data correspond to five replicate measurements after sampling on the same object at different points. One can see that both series of data can be fitted reasonably to linear graphs, consistently with the prediction from Equations (14) and (17). Remarkably, the tendency lines of 'modern' Eurocent samples differ significantly from those of the 'old' archaeological samples.

The differences between different samples are representative of the different compositions (e.g., cuprite/tenorite ratio) and/or different compactness and porosity of the corrosion layers. These properties will ultimately depend on the differences in grain shape and size distribution of the crystals of corrosion product(s) forming the

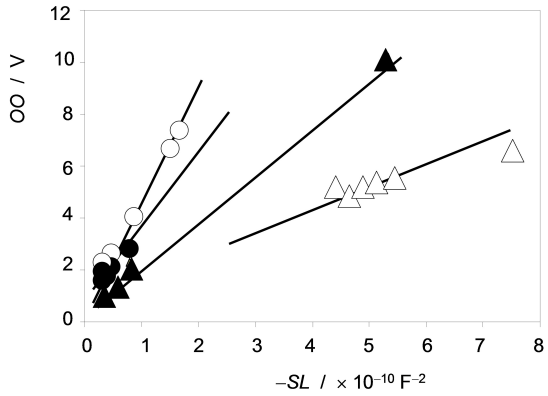

Figure 11. Plots of *OO* vs. *SL* obtained by MS analysis of impedance data recorded on Eurocent- and sample-modified graphite electrodes in contact with air-saturated 0.25 M HAc/NaAc aqueous solution at pH 4.75. Solid circles: 'fresh' Eurocent; circles: 'aged' Eurocent; solid triangles: sample 04bV57; triangles: sample 52640. Five independent measurements after sampling on different areas of the same coin are represented.

patina. As a result, a characterization of the corrosion state is obtained with obvious implications for diagnosis, conservation, tracing corrosion histories, and other archaeometric purposes such as dating.

The above treatment of impedance data can be crossed with VIMP ones assuming that we can perform successive impedance and voltammetric measurements on the same sample-modified electrode. First, we will obtain the impedance data leading to MS plots in a potential range where no faradaic processes occur. In principle, this experiment does not alter significantly the metallic sample so that the subsequent performance of VIMP (carried out in a different region of potentials where the reduction of copper corrosion products takes place) yields a second set of data for the same sample. Assuming that we perform a series of MS-VIMP sequential measurements after sampling at different depths on the same copper/bronze object, VIMP and MS parameters can be correlated. As previously noted, if the non-homogeneity of the corrosion layers is 'smooth', linear MS plots will be obtained in each individual impedance measurement.

If we perform a subsequent VIMP experiment on the same sample-modified electrode (assumed not perturbed by the previous impedance measurements), the charge passed will accomplish Equation (2), while the MS data previously taken will verify Equation (11). To correlate MS and VIMP data we can eliminate the *kS* term between Equations (1) and (11). Then, we can approximate,

$$q(1) = \frac{\sqrt{2}g\rho(1)z(1)}{\sqrt{(SL)N_D(\delta)\varepsilon(\delta)e}} \tag{30}$$

If $\rho(1)$, $z(1)$, $N_D(\delta)$, and $\varepsilon(\delta)$ can be taken as constant in replicate MS plus VIMP experiments, this equation predicts a linear variation of $\ln(q(1))$ on $\ln(SL)$ of slope −0.5.

Sequential MS-VIMP experiments produce, as expected according to the previous theoretical treatment, different values of the MS (slope, intercept) and VIMP ($i_p(1)$, $q_p(1)$) parameters upon sampling in different areas of the studied objects. Although, as can be seen in Figure 12 for samples extracted from 'fresh' and 'brown' Eurocents, and samples extracted from archaeological objects 31 and 9787. In all cases, although a relatively large dispersion appears, these data are reasonably consistent with the prediction from Equation (30), of a linear variation of $\ln q_p(1)$ on $\ln SL$. However, there

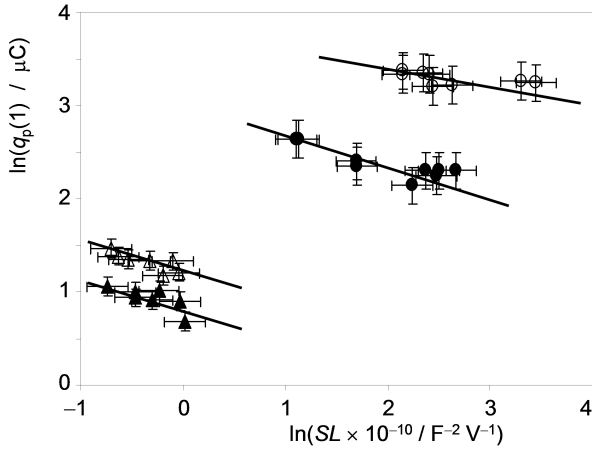

Figure 12. Plots of lnq_p(1) vs. lnSL measured, respectively, in replicate MS and VIMP experiments on samples taken on seven points of a 'fresh' (circles) and a 'brown' Eurocent (solid circles) and the objects 31 (triangles) and 9787 (solid triangles). The continuous lines correspond to the linear fit of experimental data.

is a relatively large variation of the slopes recorded for the 'fresh' Eurocent (−0.04) and 'brown' Eurocent (−0.24), and the slopes obtained for the archaeological samples, fall in the −0.30 to −0.38 range. This variation can be attributed to the different depth gradient of physicochemical properties of the corrosion patina, then producing deviations from the simplified view of Equation (30). Interestingly, the values of the slope of lnq_p(1) vs. lnSL plots increase with increasing the degree of corrosion of the metal surface and, eventually, this parameter could be an age marker under favorable conditions (equivalent composition and manufacturing type, uniform conditions of aging).

Conclusions

Attachment of nanosamples from the corrosion layers of metals to graphite electrodes, characteristic of the voltammetry of immobilized particles methodology, can be used for applying Mott-Schottky analysis of electrochemical impedance data. This requires the compensation of the impedance effect exerted by the portion of the bare graphite directly exposed to the electrolyte. The model discussed here permits this compensation and the influence of the different amounts of sample handled in each individual sampling.

The model is expanded to consider the variation of properties of the metal patina with depth. Assuming that MS data are mainly influenced by the depth variation of the density of charge carriers, two different models, exponential decay and potential decay, are developed and tested using impedance measurements for Eurocent coins in contact with an aqueous acetate buffer. Data for archaeological bronze artifacts (Etruscan culture) from the site of Pyrgi in Santa Severa (Rome, Italy) are also provided. The theoretical modeling is also developed to combine VIMP and MS data recorded in sequential experiments carried out on the same samples. Experimental data from Eurocent coins and archaeological samples show a satisfactory agreement with theoretical predictions. These results evidence the possibility of combining both electrochemical techniques for the analysis of metal corrosion processes. As the proposed methodology involves the disposal of amounts of sample at the nanogram level taken in a small area (ca. 1 mm^2 sized) area, it can be considered as interesting for local analysis and mapping in metal corrosion studies. This interest is enhanced in the archaeometric domain, where the proposed methodologies can provide relevant information concerning manufacturing techniques, corrosion history, and diagnostic criteria for conservation, tracing, and dating.

Acknowledgements

Financial support from Project PID2020-113022 GB–I00 supported by MCIN/AEI/10.13039/501100011033, Fondo Europeo de Desarrollo Regional (ERDF) and Agencia Estatal de Investigación (AEI), and Project AICO/2021/095 which is supported with Generalitat Valenciana and Fondo Europeo de Desarrollo Regional (ERDF), as well as Sapienza University of Rome (Grant in 2021, PhD and mobility award funds) is gratefully acknowledged.

Conflict of Interests

The authors declare no conflict of interest.

Data Availability Statement

The data that support the findings of this study are available from the corresponding author upon reasonable request.

Keywords: Voltammetry of immobilized particles · Mott-schottky analysis · Bronze · Corrosion

[1] *Solid State Electrochemistry I: Fundamentals, Materials, and Applications*. (Ed: V. V. Karton), Wiley, New York **2009**.
[2] C. Erinmwingbovo, M. S. Palagonia, D. Broglioli, F. La Mantia, *ChemPhysChem* **2017**, *18*, 917–925.
[3] K. Malaie, F. Scholz, U. Schröder, H. Wulff, H. Kahlert, *ChemPhysChem* **2022**, *23*, e202200364.
[4] A. Doménech-Carbó, S. López, B. Chandía, G. Cáceres, E. Muñoz, *ChemPhysChem* **2023**, *24*, 202200853.
[5] A. Doménech-Carbó, S. López, E. Muñoz, *J. Phys. Chem. C* **2024**, *128*, 1487–1495.
[6] J. J. Kelly, D. Vanmaekelbergh, *Electrochim. Acta* **1998**, *43*, 2773–2780.
[7] T. Berger, D. Monllor-Satoca, M. Jankulovska, T. Lana-Villarreal, R. Gómez, *ChemPhysChem* **2012**, *13*, 2824–2875.
[8] F. La Mantia, J. Stojadinović, M. Santamaria, F. Di Quarto, *ChemPhysChem* **2012**, *13*, 2910–2918.
[9] F. Scholz, B. Meyer, *Voltammetry of Solid Microparticles Immobilized on Electrode Surfaces, in Electroanalytical Chemistry, A Series of Advances* (Eds.: A. J. Bard, and I. Rubinstein), Marcel Dekker, New York **1998**, vol. 20, pp 1–86.
[10] F. Scholz, U. Schröder, R. Gulabowski, A. Doménech-Carbó, *Electrochemistry of Immobilized Particles and Droplets*, 2nd ed. Springer, Berlin-Heidelberg **2014**.
[11] A. Doménech-Carbó, J. Labuda, F. Scholz, *Pure Appl. Chem.* **2013**, *85*, 609–631. IUPAC Technical Report.
[12] H. Gerischer, R. McIntyre, *J. Chem. Phys.* **1985**, *83*, 1363–1370.
[13] M. H. Dean, U. Stimming, *J. Electroanal. Chem.* **1987**, *228*, 135–151.

[14] N. A. Kyerematenga, V. Hornebecq, H. Martinez, P. Knauth, T. Djenizian, *ChemPhysChem* **2012**, *13*, 3707–3713.
[15] F. Fabregat-Santiago, I. Mora-Seró, G. Garcia-Belmonte, J. Bisquert, *J. Phys. Chem. B* **2003**, *107*, 758–768.
[16] A. Doménech-Carbó, M. T. Doménech-Carbó, *Electrochemistry for Cultural Heritage*, (Eds: F. Scholz, L. Peter), Springer, Cham **2023**.
[17] A. Doménech-Carbó, M. T. Doménech-Carbó, I. Martínez-Lázaro, *Microchim. Acta* **2008**, *162*, 351–359.
[18] V. Costa, K. Leyssens, A. Adriaens, N. Richard, F. Scholz, *J. Solid State Electrochem.* **2010**, *14*, 449–451.
[19] D. Satovic, S. Martinez, A. Bobrowski, *Talanta* **2010**, *81*, 1760–1765.
[20] F. Arjmand, A. Adriaens, *J. Solid State Electrochem.* **2012**, *16*, 535–543.
[21] F. Di Turo, N. Montoya, J. Piquero-Cilla, C. De Vito, F. Coletti, G. Favero, A. Doménech-Carbó, *Anal. Chim. Acta* **2017**, *955*, 36–47.
[22] A. Doménech-Carbó, M. T. Doménech-Carbó, E. Montagna, C. Álvarez-Romero, Y. Lee, *Talanta* **2017**, *169*, 50–56.
[23] A. Doménech-Carbó, M. T. Doménech-Carbó, C. Álvarez-Romero, N. Montoya, T. Pasíes-Oviedo, M. Buendía-Ortuño, *Electroanalysis* **2017**, *29*, 2008–2018.
[24] A. Doménech-Carbó, M. T. Doménech-Carbó, C. Álvarez-Romero, T. Pasíes-Oviedo, M. Buendía-Ortuño, *Electroanalysis* **2019**, *31*, 1164–1173.
[25] M. Di Fazio, A. C. Felici, F. Catalli, M. T. Doménech-Carbó, C. De Vito, A. Doménech-Carbó, *Microchem. J.* **2020**, *152*, 104306.
[26] A. Doménech-Carbó, M. T. Doménech-Carbó, S. Capelo, T. Pasíes-Oviedo, I. Martínez-Lázaro, *Angew. Chem. Int. Ed.* **2014**, *53*, 9262–9266.
[27] L. Robbiola, J. M. Blengino, C. Fiaud, *Corros. Sci.* **1998**, *40*, 2083–2111.
[28] I. Constantinides, A. Adriaens, F. Adams, *Appl. Surf. Sci.* **2002**, *189*, 90–101.
[29] L. Robbiola, R. Portier, *J. Cult. Herit.* **2006**, *7*, 1–12.
[30] M. Serghini-Idrissi, M. C. Bernard, F. Z. Harrif, S. Joiret, K. Rahmouni, A. Srhiri, H. Takenouti, V. Vivier, M. Ziani, *Electrochim. Acta* **2005**, *50*, 4699–4709.
[31] C. Chiavari, K. Rahmouni, H. Takenouti, S. Joiret, P. Vermaut, L. Robbiola, *Electrochim. Acta* **2007**, *52*, 7760–7769.
[32] M. C. Bernard, S. Joiret, *Electrochim. Acta* **2009**, *54*, 5199–5205.
[33] A. Doménech-Carbó, M. Donnici, C. Álvarez-Romero, S. Daniele, M. T. Doménech-Carbó, *J. Solid State Electrochem.* **2021**, *25*, 195–206.
[34] A. Doménech-Carbó, M. Mödlinger, M. T. Doménech-Carbó, *J. Electroanal. Chem.* **2021**, *893*, 115336.
[35] A. Doménech-Carbó, M. Mödlinger, L. Osete-Cortina, M. T. Doménech-Carbó, *ChemElectroChem* **2023**, *10*, e202300405.
[36] A. Doménech-Carbó, M. Mödlinger, L. Osete-Cortina, M. T. Doménech-Carbó, *ChemEelectroChem* **2024**, *11*, e202300639.
[37] N. A. M. Shanid, M. A. Kadar, *Thin Solid Films* **2008**, *516*, 6245–6252.
[38] D. Jeong, W. Jo, J. Jeong, T. Kim, S. Han, M. -K. Son, H. Jung, *RSC Adv.* **2022**, *12*, 2632–2640.
[39] M. Urquidi-Macdonald, S. Real, D. D. Macdonald, *Electrochim. Acta* **1990**, *35*, 1559–1566.
[40] P. Yi, C. Dong, K. Xiao, C. Man, X. Li, *J. Electroanal. Chem.* **2018**, *809*, 52–58.
[41] O. Baka, O. Bacha, M. R. Khelladi, A. Azizi, *Bull. Mater. Sci.* **2023**, *46*, 84.
[42] Z. Ghelichkhah, G. S. Ferguson, D. D. Macdonald, S. Sharifi-Asl, *J. Electrochem. Soc.* **2021**, *168*, 041506.
[43] P. I. Kyesmen, N. Nombona, M. Diale, *Adv. Mater. Interf.* **2023**, *10*, 2300230.
[44] L. Robbiola, K. Rahmouni, C. Chiavari, C. Martini, D. Prandstraller, A. Texier, H. Takenouti, P. Vermaut, *Appl. Phys. A* **2008**, *92*, 161–169.
[45] N. Dongfang, Y. S. Al-Hamdani, M. Iannuzzi, *Electron. Struct.* **2023**, *5*, 035001.
[46] T. -F. Ye, H. Teng, *ECS Trans.* **2012**, *41*, 7–26.
[47] A. Kachmar, M. Tobis, E. Frackowiak, *ChemElectroChem* **2022**, *9*, e202200834.
[48] N. García, P. Esquinazi, J. Barzola-Quiquia, S. Dusari, *New J. Phys.* **2012**, *14*, 053015.
[49] J. D. Cohen, D. V. Lang, *Phys. Rev. B* **1982**, *25*, 5321–5350.
[50] D. V. Lang, J. D. Cohen, J. P. Harbison, *Phys. Rev. B* **1982**, *25*, 5285–5320.
[51] F. Di Quarto, S. Piazza, C. Sunseri, *Electrochim. Acta* **1990**, *35*, 99–107.
[52] F. Di Quarto, F. La Mantia, M. Santamaria, *Electrochim. Acta* **2005**, *50*, 5090–5102.
[53] M. Lovrić, F. Scholz, *J. Solid State Electrochem.* **1997**, *1*, 108–113.
[54] M. Lovrić, F. Scholz, *J. Solid State Electrochem.* **1999**, *3*, 172–175.
[55] U. Schröder, K. B. Oldham, J. C. Myland, P. J. Mahon, F. Scholz, *J. Solid State Electrochem.* **2000**, *4*, 314–324.

Manuscript received: August 15, 2024
Revised manuscript received: October 2, 2024
Accepted manuscript online: October 29, 2024
Version of record online: ■■, ■■

RESEARCH ARTICLE

Multiple-scan solid-state voltammetry and Mott-Schottky analysis of electrochemical impedance data of bronze corrosion layers are correlated via theoretical modeling incorporating the in-depth variation of compaction, porosity, and crystallinity of such layers.

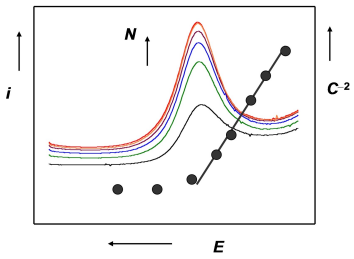

*M. Porcaro, M. Sanz-Abad, L. Michetti, A. Conti, C. De Vito, M. Teresa Doménech-Carbó, A. Doménech-Carbó**